Multimodal nonlinear optical imaging of Caenorhabditis elegans with multiplex coherent anti-Stokes Raman scattering, third-harmonic generation, second-harmonic generation, and two-photon excitation fluorescence

Shinichi Miyazaki, Philippe Leproux, Vincent Couderc, Yu Hayashi, Hideaki Kano

▶ **To cite this version:**

Shinichi Miyazaki, Philippe Leproux, Vincent Couderc, Yu Hayashi, Hideaki Kano. Multimodal nonlinear optical imaging of Caenorhabditis elegans with multiplex coherent anti-Stokes Raman scattering, third-harmonic generation, second-harmonic generation, and two-photon excitation fluorescence. Applied Physics Express, 2020, 13 (7), pp.072002. 10.35848/1882-0786/ab9711 . hal-03002626

HAL Id: hal-03002626
https://hal.science/hal-03002626v1

Submitted on 16 Nov 2020

HAL is a multi-disciplinary open access archive for the deposit and dissemination of scientific research documents, whether they are published or not. The documents may come from teaching and research institutions in France or abroad, or from public or private research centers.

L'archive ouverte pluridisciplinaire **HAL**, est destinée au dépôt et à la diffusion de documents scientifiques de niveau recherche, publiés ou non, émanant des établissements d'enseignement et de recherche français ou étrangers, des laboratoires publics ou privés.

Multimodal Nonlinear Optical Imaging of *Caenorhabditis elegans* with Multiplex Coherent Anti-Stokes Raman Scattering (CARS), Third Harmonic Generation (THG), Second Harmonic Generation (SHG), and Two-photon Excitation Fluorescence (TPEF)

Shinichi Miyazaki[1,2], Philippe Leproux[3,4], Vincent Couderc[3], Yu Hayashi[1,2,5], and Hideaki Kano[1,6,7†*]

[1]*Ph.D. Program in Humanics, University of Tsukuba, 1-1-1 Tennodai, Tsukuba, Ibaraki 305-8573, Japan*

[2]*International Institute for Integrative Sleep Medicine (WPI-IIIS), 1-1-1 Tennodai, Tsukuba, Ibaraki 305-8573, Japan*

[3]*Institut de Recherche XLIM, UMR CNRS No. 7252, 123 Avenue Albert Thomas, 87060 Limoges CEDEX, France*

[4]*LEUKOS, 37 Rue Henri Giffard, 87280 Limoges, France*

[5] *Department of Human Health Sciences, Graduate School of Medicine, Kyoto University, 53 Kawahara-cho, Shogoin, Sakyo-ku, Kyoto*

[6] *Department of Applied Physics, Graduate School of Pure and Applied Sciences, University of Tsukuba, 1-1-1 Tennodai, Tsukuba, Ibaraki 305-8573, Japan*

[7]*Department of Chemistry, Kyushu University, 744, Motooka, Nishi-ku, Fukuoka, Fukuoka 819-0395, Japan*

*Corresponding author: Hideaki Kano, E-mail: hkano@chem.kyushu-univ.jp

Multimodal nonlinear optical microscopy was used to analyze the nematode *Caenorhabditis elegans* (*C. elegans*) expressing yellow fluorescent protein (YFP) in the neurons. The lipid and protein distributions were clearly visualized using multiplex coherent anti-Stokes Raman scattering (CARS), second harmonic generation (SHG), third harmonic generation (THG), and two-photon excitation fluorescence (TPEF). The TPEF and SHG signals were found to overlap, which allowed identification of the ventral nerve cord. These findings demonstrate the powerful potential of multimodal nonlinear optical microscopy to reveal *C. elegans* microstructures *in vivo*.

Nonlinear optical imaging is a powerful method for visualizing cells and tissues *in vivo* with subcellular three-dimensional spatial resolution. Since the first description of two-photon excitation fluorescence (TPEF)[1], nonlinear optical imaging has been widely applied to biological studies, especially neurosciences[2,3]. Other nonlinear optical modalities such as coherent anti-Stokes Raman scattering (CARS)[4–10], second harmonic generation (SHG)[11–14], third harmonic generation (THG)[15,16], and third order sum frequency generation (TSFG)[17], are frequently used to visualize individual live cells and tissues. Among these nonlinear optical modalities, SHG can visualize unique noncentrosymmetric structures. Collagen[11,12], actomyosin[13], and tubulin[14] are known SHG-active proteins in organisms.

The roundworm *Caenorhabditis elegans* (*C. elegans*), a popular animal model, has been visualized using SHG and THG imaging[14–16,18]. Myosin in pharyngeal[18] and body-wall[14] muscles has been visualized by SHG imaging, whereas lipid droplets[15] and degenerated neurons[16] have been visualized by THG imaging. Microtubules in neurons are also SHG-active molecules. However, axonal microtubules in *C. elegans* have not been visualized using SHG imaging.

We previously found that ciliary rootlets that are composed of rootletin filaments[19] are SHG-active, at an intensity that is ~1,000-fold weaker than that of collagen at sclera. Moreover, we found photo-induced weak SHG signals in *centrosymmetric* polystyrene microspheres[20]. These findings indicate that our system can visualize hitherto unknown SHG-active organelles. Here, we used multimodal nonlinear optical imaging with a highly sensitive SHG channel to visualize organelles in *C. elegans*. As a result, we found that axons could be visualized without any labels. The SHG signal intensity at the axons was >10-fold weaker than that of myosin at the pharyngeal muscle. These findings indicated that our setup was sufficient for the label-free imaging of axons in *C. elegans*.

We collected multiplex CARS, THG, SHG, and TPEF signals from worms using a nonlinear optical microscope that we developed[21], with an improved and custom-made laser source, which comprised a master oscillator fiber amplifier (MOFA) with a microchip Nd: YVO_4 laser oscillator and a Yb-doped fiber amplifier (SM-1000, Leukos, Limoges, France). The wavelength, temporal duration, and repetition rate were 1064 nm, 50 ps, and 1 MHz,

respectively. The output laser beam was divided into one each for the pump beam (ω_1) for CARS and the Stokes beam (ω_2). The Stokes laser beam was prepared by introducing the 1,064-nm laser beam into a photonic crystal fiber to generate supercontinuum radiation. The pump and Stokes laser beams were superimposed by a notch filter and guided into a modified inverted microscope (ECLIPSE Ti, Nikon Corp., Tokyo, Japan). The sample was placed on a Nano-LP200 piezoelectric stage (Mad City Labs Inc., Madison, WI, USA) for position selection. The laser beams were tightly focused using a CFI Plan Apo 60x NA 1.27, water-immersion objective lens (Nikon Corp., Tokyo, Japan). The THG ($3\omega_1$), SHG ($2\omega_1$), TPEF, and multiplex CARS ($2\omega_1$-ω_2) signals were collected using a second objective lens. The THG, SHG, and TPEF signals were detected using a SpectraPro300i spectrometer (Princeton Instruments Inc., Trenton, NJ, USA) equipped with a PIXIS 100B CCD camera (Princeton Instruments), and CARS signals were identified using an LS785 spectrometer (Princeton Instruments) equipped with a BLAZE 100HR CCD camera (Princeton Instruments). The exposure time at each spatial position was 50 ms.

C. elegans Bristol N2 (wild-type) and SLP732 (remEx267[P_{H20}*::venus*]) (transgenic) worms were cultured as described[22] on agar plates containing nematode growth medium (NGM) with OP50 *Escherichia coli* at 20°. H20 is a pan-neuronal promoter[23], and Venus[24] is the yellow fluorescent protein (YFP) variant. SLP732 was generated by the standard microinjection method[25]. Briefly, the P_{H20}::venus plasmid was generated following a previous study[26] and injected into the gonad of wild-type worms. Cultured wild-type and transgenic worms were mounted on the microscope stage using transparent polydimethylsiloxane (PDMS) Worm Sheets (Biocosm Inc. Amagasaki City, Hyogo, Japan), that were developed to immobilize the worm for imaging[28].

Figure 1 shows bright-field (a), THG (b), SHG (c), TPEF (d), and CARS (e) images. The CARS image corresponds to the intensity map at the Raman shift of 2850 cm^{-1}. The width and length of the images are 50 and 150 μm, respectively. Since our primary targets were neurons, our regions of interest focused on the central nervous system of these worms. In the present experiment, transgenic worms that express Venus pan-neuronally (SLP732: remEx267[*PH20::venus*]) were used to detect neurons.

The bright-field image (Fig. 1(a)) indicated bulb and tube-like structures that

corresponded to the pharynx. The THG image (Fig. 1(b)) shows the boundaries of the pharynx and the body wall. The spectral profile of the THG signal at the cross in Fig. 1(b) is colored light blue in Fig. 1(f), in which a sharp spectral profile due to a THG signal was identified at 355 nm. Since THG gives contrast at the boundaries or interfaces between two objects with different refractive indices, this image reflects the boundaries of anatomical structures in the worm, such as the pharyngeal stroma and muscles. The THG image also shows some droplet-like structures around the gut (Fig. 1(b)). Some droplets emitted an intense CARS signal at 2,850 cm^{-1} (Fig. 1(g)), which is assigned to the CH_2 symmetric stretching vibrational mode. Therefore, droplets with high THG activity are ascribable to lipid droplets in the intestine, and their distribution was consistent with previous findings[29]. The SHG image around the head of the worm shows a strong SHG signal around the pharynx, which is saturated (Fig. 1(c)). Considering that the pharynx mainly comprises of muscle cells and that SHG signals derived from pharyngeal myosin have been reported[18], the SHG-active area around the center in Fig. 1(c) was safely assigned to muscle myosin. In addition to the intense SHG signal in the pharynx, a filamentous structure was evident around the pharynx (visible only at the right side in Fig. 1(c)). Based on a previous study[30], collagen and tubulin in neuronal axons are plausible candidates for SHG-active filaments. Indeed, the anatomical features of the filamentous structure seemed to match well with the ventral nerve cord (VNC)(detailed schematics are discussed below, and Fig. 4(e) shows the VNC). Since the VNC of this worm was labeled with Venus, the position of the VNC was visualized by two-photon excitation fluorescence (TPEF) using the same laser source. Figure 1(d) shows the TPEF image of Venus. We found that the fluorescence signal due to Venus and the SHG signals were simultaneously detected and spectrally overlapped (Fig. 1(f), light green), further supporting that the SHG-active structures would be assigned as axons. We sorted these spectrally overlapping signals into two components as follows. Figure 1(f) shows a sharp SHG signal at 532 nm. We first fitted the spectral profile of the SHG signal using a Gaussian curve with a fluorescent background. The amplitude of the fitted Gaussian curve was then mapped, and the SHG image was reconstructed (Fig. 1(c)). On the other hand, the spectral profile of the TPEF signal was broad and asymmetric. Therefore, we integrated the TPFE signal intensity from 900 to 928 nm and subtracted the contribution of the SHG signal from it (Fig. 1(d)). The TPEF image clearly indicates the location of the VNC on the right

side of the worm. Figure 1(e) shows a CARS image at the Raman shift of 2,850 cm^{-1} (Fig. 1(g); black arrow). The CARS signal was also evident at the polymer chamber used for immobilizing the worms, which is addressed in Fig. 3.

Next, we obtained a sectional (XZ) image (width and height, 25 × 25 μm) of the worm (Fig. 2). We used a different microscope objective lens (LD C-APOCHROMAT 63x NA 1.15, Carl Zeiss Microscopy GmbH, Jena, Germany) for sectional imaging because the depth resolution is found to be improved, though the transmissivity of the pump and Stokes is worse. The THG image (Fig. 2(a)) shows two boundaries at the bottom. The THG intensity profile, along with z position, is shown in the left panel of the THG image. Since we used a buffer to load the worms, there were three different materials, the glass coverslip, buffer, and polymer chamber (as shown in Fig. 2(c)). As these materials have different refractive indices, there were two boundaries (Fig. 2(a)). We estimated the depth (axial) resolution of our system based on the experimental results shown in the THG image. The THG intensity profile shown in Fig. 2(a) was fitted by the sum of Gaussian curves. The calculated full width at half maxima (FWHM) of two Gaussian curves were 1.6 ± 0.4 and 2.6 ± 0.2 μm for the interfaces between the cover glass and buffer, and between the buffer and chamber, respectively. Several bright spots visualized around the center of the roundworm might have reflected the inner lumen of the pharynx.

The depth-resolved SHG image shows a ring-like structure in the body of the roundworm (Fig. 2(b)), and Fig. 1(c) shows an intense SHG signal at the pharynx muscle. The position of the roundworm in Fig. 2 was around the posterior bulb of the pharynx surrounded by the pharyngeal muscles. Therefore, the SHG-active ring-like structures were due to myosin in the pharyngeal muscles. We also estimated the depth resolution of SHG imaging. We evaluated the upper limit by fitting the bright spot using a Gaussian curve. The fitted FWHM was 2.4 ± 0.1 μm, which was similar to those obtained by THG imaging. Based on these results, the estimated axial (depth) resolution of the UV-visible signal was about < 2.5 μm under our experimental conditions.

We analyzed the spectrum of the CARS signal to determine the details of the molecular distribution in the body of the worm. The $\mathrm{Im}[\chi^{(3)}]$ spectrum at each spatial position

was calculated from raw CARS spectra using the maximum entropy method (MEM)[31,32]. This method does not require any *a priori* knowledge of the vibrational band, and can retrieve phase information on third order nonlinear susceptibility $\chi^{(3)}$, the imaginary part of which corresponds to the spontaneous Raman spectrum. The spectral profiles of the Im[$\chi^{(3)}$] signal were then fitted by the sum of the Gaussian curves, and the amplitudes of the Gaussian curves were mapped. Figures 3(a)-(f) show the CARS (Im[$\chi^{(3)}$]) images at the Raman shifts of 2,960, 2,930, 2,850, 1,650, 1,450, and 705 cm^{-1}, which were assigned to the CH_3 asymmetric stretching, CH_3 stretching, CH_2 stretching, *cis* C=C stretching, CH_3 degenerate deformation, and Si-C asymmetric stretching vibrational modes, respectively. Typical spectral profiles of the Im[$\chi^{(3)}$] signal at 2,960, 2,930, 2,850, 1,655, 1,450, 1,003, and 705 cm^{-1} are shown in Fig. 3(g) at the spatial points indicated in Fig. 3(a). The Im[$\chi^{(3)}$] spectra of the worm were superimposed by that of the surrounding polymer chamber. Characteristic bands due to the polymer were evident around 705 and 2,960 cm^{-1}. According to a previous study on PDMS[33], the Raman bands at 705 cm^{-1}, and 2,960 cm^{-1} were assigned to Si-C and CH_3 asymmetric stretching vibrational modes, respectively. Since the CARS signal at the CH stretching vibrational mode was saturated at the polymer chamber, MEM cannot be applied from 2930 to 1780 cm^{-1} (Fig. 3(g), light green). Figure 3(c) shows several bright spots, mainly in the intestine, and there are some bands in the spectral profile at the bright spot (Fig. 3(g), red). The Raman bands at 2,930, 2,850, and 1,655 cm^{-1} were assigned to lipids, indicating that lipid droplets are stored in the intestine (Figs. 3(b)-(d)). Figure 3(b) and Fig. 3(e) show CARS(Im[$\chi^{(3)}$]) images at the Raman band of 2930 cm^{-1} (CH_3 stretching) and 1450 cm^{-1} (degenerate deformation). These bands were mainly located protein-rich regions such as the pharynx and directly below the cuticle.

We merged images of the SHG (green) and TPEF (yellow) signals to further investigate their co-localization (Fig. 4(a)). Merged and magnified images (Figs. 4(b) and (c)) show an SHG-active structure located around the pharynx, and that it was Venus-labeled. We also evaluated the wild-type roundworm using SHG imaging (Fig. 4(d)). The SHG signal indicated a similar filamentous structure without a label. Figure 4(e) shows a schematic of the anatomical structure around the pharynx of the roundworm, nerve ring, dorsal nerve cord (DNC), and VNC. Since the VNC contained more axons than the DNC and the direction of

axons in VNC is almost identical, the SHG signal should be more significant at the VNC than at the nerve ring or the DNC. A previous study did not find an SHG signal in the roundworm tail[34], which might have been due to the tail having far fewer axons than the VNC. The present study also did not identify an SHG signal at the tail (data not shown).

In conclusion, we visualized internal fine structures of *C. elegans* using multimodal nonlinear optical microscopy. The THG image indicated lipid distribution in the worms, which was supported by the multiplex CARS signals. We found SHG signals not only at sites of myosin but also around axons. The visualized axons were confirmed by the colocalized SHG and TPEF signals. These results indicated that nonlinear optical imaging is a promising method with which to visualize biomolecules in *C. elegans in vivo*. Moreover, the SHG signal can visualize unlabeled axons.

Acknowledgments

This study was financially supported by JSPS KAKENHI Grant Number 18H02000(Grant-in-Aid for Scientific Research [B] to H.K.) and Japan Science and Technology Agency Grant Number JPMJCR1655 (to Y.H.). The authors are grateful to J. Ukon of Ukon Craft Science, Ltd. for establishing this collaboration between Japanese and French laboratories, and to Professor T. Hattori for fruitful discussions regarding nonlinear optics.

References

[1] W. Denk, J.H. Strickler, and W.W. Webb, Science (80-.). **248**, 73 (1990).

[2] R. Yuste and W. Denk, Nature (1995).

[3] S. K, D. W, K. D, and T. Dw, Nature **385**, 161 (1997).

[4] J.X. Cheng, A. Volkmer, L.D. Book, and X.S. Xie, J. Phys. Chem. B **106**, 8493 (2002).

[5] C.H. Camp, Y.J. Lee, J.M. Heddleston, C.M. Hartshorn, A.R.H. Walker, J.N. Rich, J.D. Lathia, and M.T. Cicerone, Nat. Photonics **8**, 627 (2014).

[6] M. Müller and J.M. Schins, J. Phys. Chem. B **106**, 3715 (2002).

[7] T.W. Kee and M.T. Cicerone, Opt. Lett. **29**, 2701 (2004).

[8] H. Kano and H. Hamaguchi, Appl. Phys. Lett. **86**, 1 (2005).

[9] G.I. Petrov and V. V. Yakovlev, Opt. Express **13**, 1299 (2005).

[10] E.R. Andresen, H.N. Paulsen, V. Birkedal, J. Thøgersen, and S.R. Keiding, J. Opt. Soc. Am. B (2005).

[11] I. Freund and M. Deutsch, Opt. Lett. **11**, 94 (1986).

[12] S. Fine and W.P. Hansen, Appl. Opt. (1971).

[13] V. Nucciotti, C. Stringari, L. Sacconi, F. Vanzi, L. Fusi, M. Linari, G. Piazzesi, V. Lombardi, and F.S. Pavone, Proc. Natl. Acad. Sci. U. S. A. **107**, 7763 (2010).

[14] P.J. Campagnola, A.C. Millard, M. Terasaki, P.E. Hoppe, C.J. Malone, and W.A. Mohler, Biophys. J. **82**, 493 (2002).

[15] D. Fu, W. Yang, and X.S. Xie, 27 (2017).

[16] E.J. Gualda, G. Filippidis, G. Voglis, M. Mari, C. Fotakis, and N. Tavernarakis, J. Microsc. **229**, 141 (2008).

[17] H. Segawa, M. Okuno, H. Kano, P. Leproux, V. Couderc, and H. Hamaguchi, **20**, 11014 (2012).

[18] E.J. Gualda, G. Filippidis, G. Voglis, M. Mari, C. Fotakis, and N. Tavernarakis, Opt. InfoBase Conf. Pap. (2007).

[19] T. Akiyama, A. Inoko, Y. Kaji, S. Yonemura, K. Kakiguchi, H. Segawa, K. Ishitsuka, M. Yoshida, O. Numata, P. Leproux, V. Couderc, T. Oshika, and H. Kano, Sci. Rep. **7**, 1 (2017).

[20] K. Makihara, D. Kaneta, T. Iwamura, A. Sugita, P. Leproux, V. Couderc, and H. Kano, Appl. Phys. Express (2020).

[21] H. Yoneyama, K. Sudo, P. Leproux, V. Couderc, A. Inoko, and H. Kano, APL Photonics **092408**, (2018).

[22] S. Brenner, Genetics **77**, 71 (1974).

[23] G. Shioi, M. Shoji, M. Nakamura, T. Ishihara, I. Katsura, H. Fujisawa, and S. Takagi, Genetics **157**, 1611 (2001).

[24] T. Nagai, K. Ibata, E. Park, M. Kubota, and K. Mikoshiba, Nat. Biotechnol. **20**, 1585 (2002).

[25] C.C. Mello, J.M. Kramer, D. Stinchcomb, and V. Ambros, EMBO J. (1991).

[26] Y. Hayashi, T. Hirotsu, R. Iwata, E. Kage-Nakadai, H. Kunitomo, T. Ishihara, Y. Iino, and T. Kubo, Nat. Neurosci. (2009).

[27] T. Nagai, K. Ibata, E.S. Park, M. Kubota, K. Mikoshiba, and A. Miyawaki, Nat. Biotechnol. (2002).

[28] M. Suzuki, T. Sakashita, Y. Hattori, Y. Yokota, Y. Kobayashi, and T. Funayama, J. Neurosci. Methods **306**, 32 (2018).

[29] C. Brackmann, P. Hillertz, M. Pilon, A. Enejder, T. Hellerer, and C. Axa, 1 (2007).

[30] F.S. Pavone and P.J. Campagnola, *Second Harmonic Generation Imaging* (2013).

[31] E.M. Vartiainen, H.A. Rinia, M. Müller, and M. Bonn, Opt. Express **14**, 3622 (2006).

[32] M. Okuno, H. Kano, P. Leproux, V. Couderc, J.P.R. Day, M. Bonn, and H. Hamaguchi, Angew. Chem. Int. Ed. **49**, 6773 (2010).

[33] D. Cai, A. Neyer, R. Kuckuk, and H.M. Heise, J. Mol. Struct. **976**, 274 (2010).

[34] G. Filippidis, C. Kouloumentas, G. Voglis, F. Zacharopoulou, T.G. Papazoglou, and N. Tavernarakis, J. Biomed. Opt. **10**, 024015 (2005).

Figure Captions

Fig. 1. Bright-field (a), THG (b), SHG (contribution of fluorescence signal was subtracted) (c), TPEF (Venus, a YFP variant; contribution of SHG signal was subtracted) (d), and CARS (at 2,850 cm^{-1}) (e). Spectral profiles of THG, SHG and TPEF at crosses in (b) (light blue) and (c) (light green) (f) and of CARS signal (g) at cross in (e). Intensity is shown as arbitrary units in (f) and (g).

Fig. 2. Sectional images of THG (a) and SHG (b). Schematics of mounted worm (c) surrounded by polydimethylsiloxane (PDMS) chamber and buffer.

Fig. 3. CARS images at 2,960 (a), 2,930 (b), 2,850 (c), 1,650 (d), 1,450 (e), and 705 (f) cm^{-1}. CARS spectrum profiles (g) at spatial points indicated in (a). The spectral dip indicated as "*" are an artifact due to CARS spectral correction, through which CARS signal at each spatial point was divided by nonresonant background of coverslip underneath the roundworm (g).

Fig. 4. SHG and TPEF merged image (a), SHG image (enlarged) (b), TPEF image (enlarged) (c), SHG image of wild-type worm (d). schematics of neurons around the pharynx (e). Triangle indicates the structure related to the axons. The direction of the worm is identical in all images.

Fig. 1

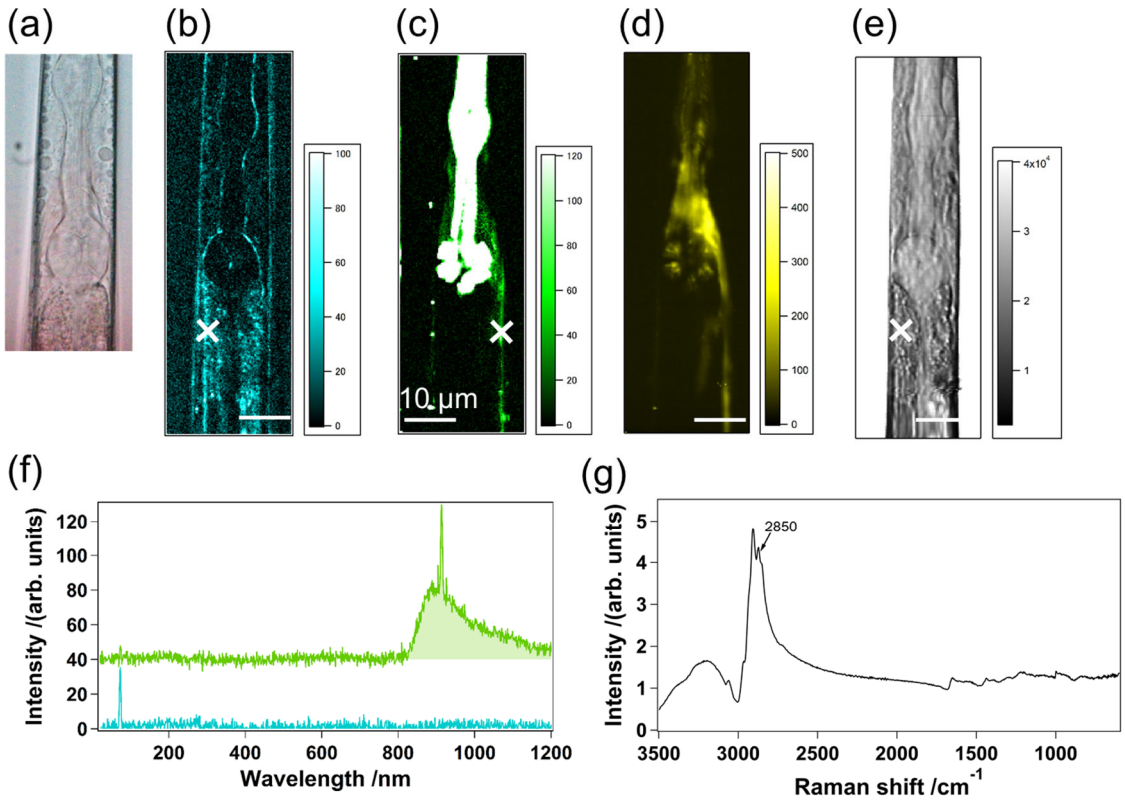
(a)
(b)
(c)
(d)
(e)
10 μm
(f)
Intensity /(arb. units)
Wavelength /nm
(g)
2850
Intensity /(arb. units)
Raman shift /cm-1

Fig. 2

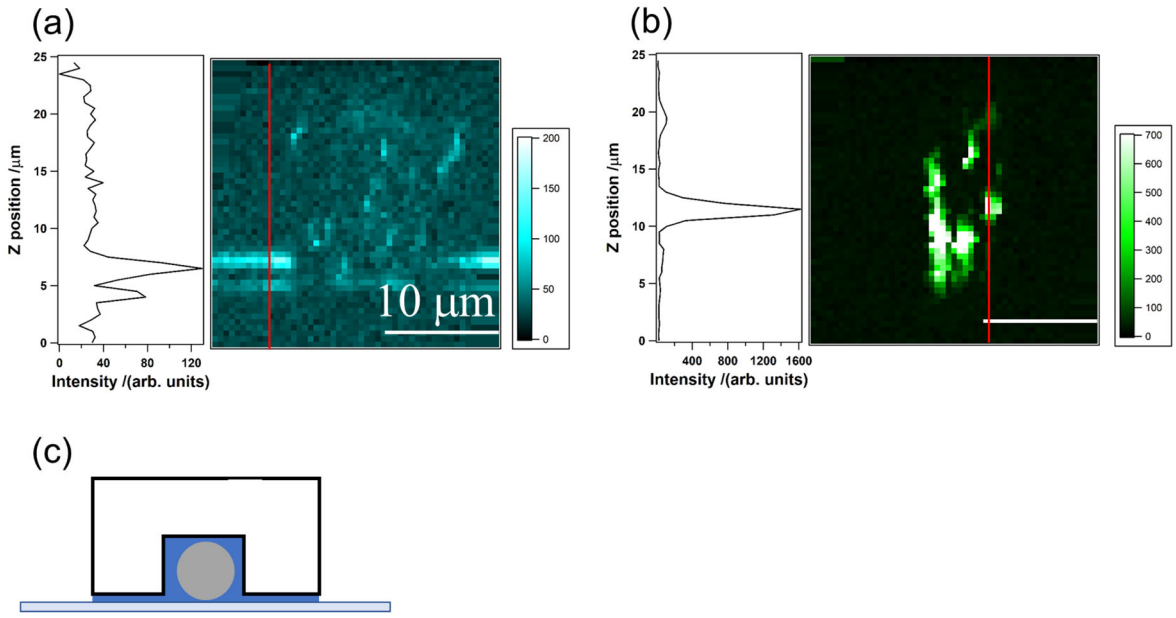
(a)
Z position /μm
Intensity /(arb. units)
10 μm
(b)
Z position /μm
Intensity /(arb. units)
(c)

Fig. 3

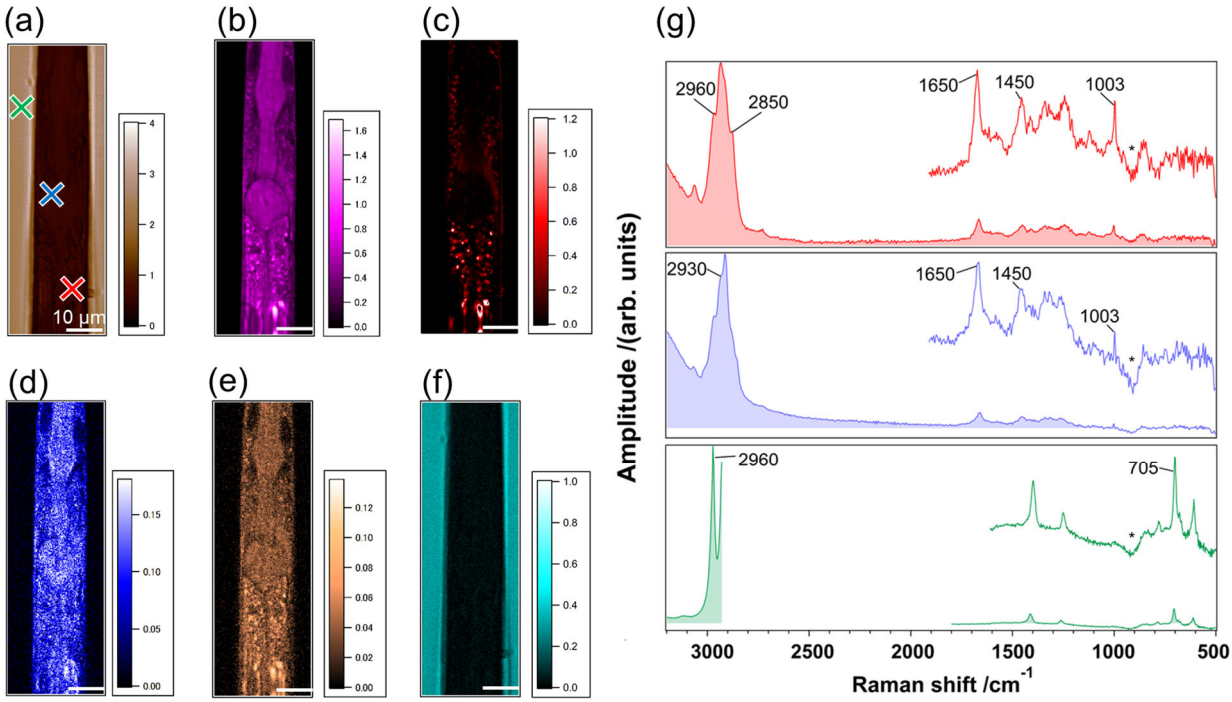
(a)
(b)
(c)
(d)
(e)
(f)
(g)
10 μm
2960
2850
1650
1450
1003
2930
705
Amplitude /(arb. units)
Raman shift /cm-1
3000
2500
2000
1500
1000
500

Fig. 4

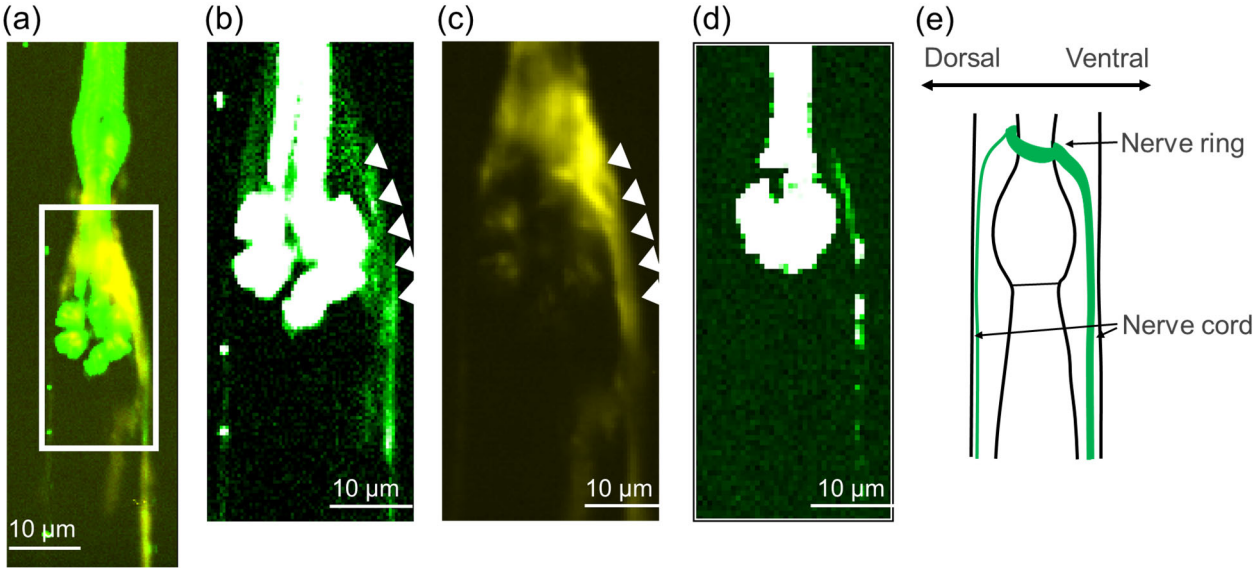
(a)
(b)
(c)
(d)
(e)
10 μm
10 μm
10 μm
10 μm
Dorsal
Ventral
Nerve ring
Nerve cord